



Summertime changes in climate extremes over the peripheral Arctic regions after a sudden sea ice retreat

Steve Delhay¹, Thierry Fichefet¹, François Massonnet¹, David Docquier², Rym Msadek³, Svenya Chripko³, Christopher Roberts⁴, Sarah Keeley⁴, and Retish Senan⁴

¹Georges Lemaître Centre for Earth and Climate Research, Earth and Life Institute, Université catholique de Louvain, Louvain-la-Neuve, Belgium

²Royal Meteorological Institute of Belgium, Brussels, Belgium

³CECI, Université de Toulouse, CNRS, CERFACS, Toulouse, France

⁴European Centre for Medium-Range Weather Forecasts, Shinfield Park, Reading, RG2 9AX, UK

Correspondence: Steve Delhay (steve.delhay@uclouvain.be)

Abstract. The retreat of Arctic sea ice is frequently considered as a possible driver of changes in climate extremes in the Arctic and possibly down to mid-latitudes. However, it is unclear how the atmosphere will respond to a near-total retreat of summer Arctic sea ice, a reality that might occur in the foreseeable future. This study explores this question by conducting sensitivity experiments with two global coupled climate models run at two different horizontal resolutions to investigate the change in temperature and precipitation extremes during summer over peripheral Arctic regions following a sudden reduction in summer Arctic sea ice cover. An increase in frequency and persistence of maximum surface air temperature is found in all peripheral Arctic regions during the summer when sea ice loss occurs. For each million km² of Arctic sea ice extent reduction, the absolute frequency of days exceeding the surface air temperature of the climatological 90th percentile increases by ~4% over the Svalbard area, and the duration of warm spells increases by ~1 day per month over the same region. Furthermore, we find that the 10th percentile of surface daily air temperature increases more than the 90th percentile, leading to a weakened diurnal cycle of surface air temperature. Finally, an increase in extreme precipitation, which is less robust (statistically speaking) than the increase in extreme temperatures, is found in all regions in summer. These findings suggest that a sudden retreat of summer Arctic sea ice clearly impacts the extremes in maximum surface air temperature and precipitation over the peripheral Arctic regions with the largest influence over inhabited islands such as Svalbard or Northern Canada. Nonetheless, even with a large sea ice reduction in regions close to the North Pole, the local precipitation response is relatively small compared to internal climate variability.

1 Introduction

Arctic sea ice extent has been decreasing since the beginning of satellite observations in 1979. This decrease has occurred in all seasons but is more pronounced during summer. Actually, September sea ice extent has shrunk by about 50% since the beginning of the satellite era (Onarheim et al., 2018). Moreover, sea ice in the central Arctic has become thinner, with a reduction in ice thickness of about 65% between 1975 and 2012 (Lindsay and Schweiger, 2015). Ice thickness has decreased



much faster than previously predicted in several marginal seas (Mallett et al., 2021). The loss of sea ice, which is largely attributed to the accumulation of greenhouse gases in the atmosphere following anthropogenic emissions (Notz and Stroeve, 2016; Screen et al., 2018) but also to internal climate variability (Ding et al., 2017), has been proposed as a key driver of the "Arctic Amplification" (AA) through changes in albedo (Manabe and Stouffer, 1994; Screen and Simmonds, 2010) and other temperature-related feedbacks (Pithan and Mauritsen, 2014).

The signature of AA on the state of the atmosphere is clearly evident, with a warming at high latitudes at least twice as high as at low latitudes (Serreze et al., 2009; Screen and Simmonds, 2010; Cowtan and Way, 2014; Ballinger et al., 2020). AA associated to Arctic sea ice loss primarily impacts high latitudes but it could also impact lower latitudes. Indeed, it might affect the polar jet stream, the storm track and the planetary wave activity (Cohen et al., 2014) mainly during winter. These modifications could lead to more extreme mid-latitude weather, such as cold spells or droughts, through an increase of atmospheric blocking events (e.g. Francis and Vavrus, 2012; Cohen et al., 2014; Mori et al., 2014; Francis, 2017; Cohen et al., 2020). Nonetheless, the existence of a mid-latitude climate response to AA and/or Arctic sea ice loss, which has generated a lot of attention, is still debated (Ogawa et al., 2018).

To investigate the role of the sea ice retreat on climate, observations alone are not sufficient (Smith et al., 2019). Indeed, sea ice and atmospheric circulation might be related to each other in the observational record, but this relationship could have occurred by chance. The relationship could also be non-causal, especially if both sea ice and the atmospheric circulation are driven by the same confounding factor (Blackport et al., 2019). To overcome these problems, the use of numerical model experiments, in which a retreat of summer Arctic sea ice can be imposed, is an attractive approach to determine the influence of sea ice anomalies on the climate system. However, even with exactly the same experimental setup, significant differences in the mid-latitude responses are found within the same model, suggesting that internal climate variability can play a large role (Peings et al., 2021). Furthermore, other recent studies show that future mid-latitude climate response to polar forcing in the Northern Hemisphere (AA and/or sea ice loss) is weaker than initially expected (Blackport and Screen, 2020; Dai and Song, 2020).

The climate response near the regions of Arctic sea ice loss depends primarily on the surface heat flux changes (e.g. Deser et al., 2010) and is therefore less dependent on the internal climate variability than at mid-latitudes. Thereby, the signal (response of the atmosphere to sea ice loss) to noise (internally generated variability) ratio over the peripheral Arctic regions is larger and less ensemble members are needed to get a significant response compared to mid-latitude regions (Screen et al., 2014). Furthermore, less attention was paid to the summertime changes compared to the wintertime changes to Arctic sea ice loss (or AA) (e.g., Francis and Vavrus, 2012; Cohen et al., 2014; Barnes and Screen, 2015; Cohen et al., 2020).

An increase of climate extremes (frequency, intensity or persistence) impacts more human activities and the natural environment than an increase in the climatic mean (Kunkel et al., 1999). However, change in the mean climate is already impacting



the Arctic regions with a change in fish stocks (Hollowed et al., 2013; Haug et al., 2017) and in agriculture (Stevenson et al., 2014), and posing risks to local communities (Ford et al., 2008). In the 21st century, a larger decrease of magnitude in cold extremes compared to the increase in warm extremes and an increase in precipitation extremes are expected over high latitudes (Kharin et al., 2013; Sillmann et al., 2013b). The projected Arctic sea ice loss can be responsible for this decrease in temperature variance (Blackport et al., 2021) and in the increase in precipitation extremes, but with a significant difference between regions (Screen et al., 2015).

Even if the rate of summer Arctic sea ice decline is not uniform and might be slowed down for a few years depending on the effect of internal climate variability (Swart et al., 2015), sudden reductions in Arctic sea ice extent are likely to be more frequent in the future with sea ice retreating 4 times faster than the long-term trend (Holland et al., 2006). Moreover, many state-of-the-art climate models project a summer ice-free Arctic conditions before 2050 (SIMIP, 2020). The peripheral Arctic regions will be the first regions to be affected by a sudden sea ice retreat.

In this study, we investigate how the maximum surface air temperature and precipitation extremes over the Arctic regions in summer respond to a large sudden Arctic sea ice loss. To answer this question, outputs from two coupled general circulation models (GCMs) that participated in the High Resolution Model Intercomparison Project (HighResMIP; Haarsma et al. (2016)), at two different horizontal resolutions, and contributing to the EU Horizon 2020 PRIMAVERA project (PRocess-based climate sIMulation : AdVances in high resolution modelling and European climate Risk Assessment, <https://www.primavera-h2020.eu/>) are used. Although the models are quite similar in their configurations, using two models and two different horizontal resolutions allows to have a better approach to determine robust climate responses. The focus is on summer as it is the period when maximum temperatures and precipitation are highest over the peripheral Arctic regions.

The paper is organized as follows. Sect. 2 describes the two GCMs used and the experiments that have been performed in this study as well as a description of the eight climate extremes indices and areas that are used. In Sect. 3, the effect of an abrupt summer Arctic sea ice loss on the maximum surface air temperature and precipitation extremes over peripheral Arctic regions is analysed. Finally, Sect. 4 includes a summary of the results and conclusions.

2 Models and method

2.1 Models

Two fully coupled atmosphere-land-sea ice-ocean GCMs, namely, ECMWF-IFS and CNRM-CM6-1, are used in this study and described below. These models participated in the HighResMIP, which was an endorsed sub-project of the sixth phase of Coupled Model Intercomparison Project (CMIP6; Eyring et al., 2016). The model characteristics for each resolution are given in Table 1.



2.1.1 ECMWF-IFS

The atmospheric component of ECMWF-IFS, the Integrated Forecasting System (IFS), uses a semi-implicit, semi-Lagrangian discretization (Ritchie et al., 1995; Temperton et al., 2001). The model is based on the IFS cycle 43r1. The land surface component is the Hydrology Tiled ECMWF Scheme of Surface Exchanges over Land (H-TESSEL; Balsamo et al. (2009)). The ocean component is version 3.4 of the Nucleus for European Modelling of the Ocean (NEMO3.4; Madec et al., 2013). NEMO3.4 is coupled to the second version of the Louvain-la-Neuve Sea-Ice Model (LIM2; Bouillon et al. (2009); Fichefet and Morales Maqueda (1997)), which includes a three-layer model for the vertical conduction of heat in sea ice. The coupling between the ocean and atmosphere is resolved by the sequential single-executable strategy used by Mogensen et al. (2012) at a frequency of 1 hr (Roberts et al., 2018). There is no coupling between precipitation over land and the runoff to the ocean but, to overcome this limitation, a climatological approximate calculation of the freshwater input is determined at each coastal grid point. Finally, unlike the operational setup of ECMWF where the surface energy balance is calculated in the land surface module (Mogensen et al., 2012), the skin temperature from LIM2 is coupled to mitigate the excessive sea ice volume in the Arctic.

Two different configurations of the model have been used. The first configuration, ECMWF-IFS-LR (hereafter ECMWF-LR), uses the Tco199 grid for the atmosphere, which has a horizontal resolution of about 50 km, and the ORCA1 tripolar grid for the ocean, which has a nominal resolution of $\sim 1^\circ$ (Roberts et al., 2018). The second configuration, ECMWF-IFS-HR (hereafter ECMWF-HR), uses the Tco399 grid for the atmosphere, which has a horizontal resolution of about 25 km, and the ORCA025 tripolar grid for the ocean, which has a resolution of $\sim 0.25^\circ$. The vertical resolution is the same for both configurations, with 91 levels in the atmosphere, extending up to 0.01 hPa, and 75 levels in the ocean (Madec, 2016). Beside the resolution, the only differences between the two configurations come from the resolution-dependent parameterizations in NEMO (Roberts et al., 2018).

2.1.2 CNRM-CM6-1

The atmospheric component of CNRM-CM6-1 is version 6.3 of the global atmospheric model ARPEGE-Climat (Voldoire et al., 2019). It uses a semi-Lagrangian numerical integration scheme and has 91 vertical levels with a high-top level at 0.01 hPa. The model is based on cycle 37 of the ARPEGE/IFS system. This model is coupled to the surface component SURFEX, which shares the same grid and time step (Masson et al., 2013). The ocean component is NEMO3.6 (Madec et al., 2017), which includes 75 vertical levels. The sea ice component is Gelato 6 which is embedded into the ocean component. Gelato 6 uses five ice thickness categories, in which each category treats the snow as a single layer, while ice is simulated with a nine-layer vertical discretization (Voldoire et al., 2019). The coupling between the atmosphere and ocean-sea ice components is performed using the OASIS3-MCT software (Craig et al., 2017) at a 1hr frequency.



122 The first configuration, CNRM-CM6-1 (hereafter CNRM-LR), uses the T1127 grid for the atmosphere, which has a nominal
 123 horizontal resolution of 130 km, and the eORCA1 horizontal grid for the ocean (Table 1), which is an extension of the ORCA1
 124 tripolar grid that differs from ORCA1 by the use of two quasi-isotropic bipolar grids south of 67° S instead of the former
 125 Mercator grid (Voldoire et al., 2019). The second configuration, CNRM-CM6-1-HR (hereafter CNRM-HR), uses the T1359
 126 grid for the atmosphere, which has a nominal horizontal resolution of 50 km, and the eORCA025 horizontal grid for the ocean.
 127 The vertical resolutions are similar for both configurations and both components (atmosphere and ocean).
 128

Table 1. Characteristics of the two models at two different resolutions used in this study.

	ECMWF-LR	ECMWF-HR	CNRM-LR	CNRM-HR
Atmosphere				
Model	IFS cycle 43r1		ARPEGE	
Grid name	Tco199	Tco399	T1127	T1359
Nominal resolution (km)	50	25	130	50
Resolution at 50°N (km)	50	25	142	50
Vertical levels	91	91	91	91
Ocean				
Model	NEMO3.4		NEMO3.6	
Grid name	ORCA1	ORCA025	eORCA1	eORCA025
Resolution	1°	0.25°	1°	0.25°
Vertical levels	75	75	75	75
Sea ice				
Model	LIM2		Gelato 6	
Ice thickness categories	1		5	

129 2.2 Experiments

130 Two different experiments are conducted with each model configuration and follow the protocol defined within the PRIMAV-
 131 ERA project. The first experiment, the control run (CTRL), has a constant forcing corresponding to year 1950 and is run for 100
 132 years without including 30 years of spin-up, which are not analysed in this study. This control run is similar to the control-1950
 133 simulation of HighResMIP (Haarsma et al., 2016). The second experiment, the perturbation run (PERT), has the same constant
 134 forcing as CTRL but with a modified sea ice albedo. In the PERT experiment, the sea ice albedo values (dry snow, melting
 135 snow, bare frozen ice and bare puddled ice) are reduced to the open ocean value (~ 0.07) from the first model time step (1st
 136 January) and are kept equal to this value through the whole model integration to achieve a large Arctic sea ice loss in summer.



137 This perturbation increases the absorption of solar radiation and generates a melting of the snow over sea ice and of the sea ice
 138 itself. This method has already been applied in previous studies but on much longer time scales (Deser et al., 2015; Blackport
 139 and Kushner, 2016, 2017; Park et al., 2018) and produces consistent climate responses compared to other methods (Screen
 140 et al., 2018). The PERT experiment is run for 15 months only as our study focuses on the short-term climate response to Arctic
 141 sea ice loss. Moreover, in order to sample the internal climate variability, 40 members are performed in the PERT experiment,
 142 where each member starts from a different year of CTRL. This number of members was chosen because it allows to reach a
 143 good level of statistical significance in high latitudes (Screen et al., 2014) without having too long process time. One member is
 144 launched every year from CTRL with ECMWF-LR and ECMWF-HR, every two years with CNRM-HR, and every three years
 145 with CNRM-LR. As the difference between PERT and CTRL is only a change in sea ice, comparing them enables to isolate
 146 the effect of sea ice loss. To perform our analysis, we compare each member of PERT to the member of its corresponding year
 147 in CTRL (PERT-CTRL). The atmospheric responses are scaled by the amount of Arctic sea ice loss averaged over the summer
 148 (July, August and September here). Finally, the statistical significance of the atmospheric response, shown in maps, has been
 149 estimated using a two-sample Kolmogorov-Smirnov test accounting for the False Discovery Rate (FDR) (Wilks, 2016). The
 150 FDR method was first described by Benjamini and Hochberg (1995) and enables to reject local null hypotheses that are in fact
 151 true. Indeed, the rejection of the null hypothesis is valid if the p values are not larger than a threshold level (10%) that depends
 152 on the distribution of the sorted p values (Wilks, 2016) obtained here thanks to a two-sample Kolmogorov-Smirnov test.

153

154 2.3 Climate extreme indices

155 To determine the changes in extreme climate events, twenty-seven climate extreme indices have been defined by the Expert
 156 Team on Climate Change Detection and Indices (ETCCDI) created by the World Climate Research Programme (WCRP).
 157 These indices are mainly used in historical climate model simulations (e.g., Sillmann et al., 2013a) and in model projections
 158 forced by greenhouse gas emission increases (Sillmann et al., 2013b). Eight climate extreme indices of the ETCCDI are used
 159 in this study. These indices have been selected because they can show extreme changes in frequency or in persistence in sur-
 160 face air temperature or in precipitation even over high latitude regions. Four indices are based on the maximum daily surface
 161 air temperature : the frequency of cold days (TX10p : % of days over the summer period when the maximum temperature is
 162 below the 10th percentile of the CTRL), the frequency of warm days (TX90p : % of days over the summer period when the
 163 maximum temperature exceeds the 90th percentile of the CTRL), the warm spell duration index (WSDI : number of days over
 164 the summer period with at least 6 consecutive days when the maximum temperature exceeds the 90th percentile of the CTRL)
 165 and the ice days (ID : number of days over the summer period when the maximum temperature remains below 0°C). The last
 166 four indices are based on the daily precipitation : the maximum 1 day precipitation (RX1day : the maximum 1 day value of
 167 precipitation over the summer period), the wet-day precipitation (R95p : total amount of precipitation during wet days (>1mm)
 168 for days where precipitation exceeds the 95th percentile of the CTRL over the summer period), the consecutive dry days (CDD
 169 : maximum number of consecutive days over the summer period when the daily precipitation does not exceed 1mm) and the
 170 consecutive wet days (CWD : maximum number of consecutive days over the summer period when the daily precipitation ex-



ceeds 1mm). More details are given below or can be found in Zhang et al. (2011) or in Sillmann et al. (2013a) for all the indices.

For each calendar day, the values of the 10th (for TX10p) and 90th percentiles (for TX90p and WSDI) of the 40-yr period CTRL centered on a 5 day window are first calculated (the vertical blue lines in Fig. 1 on August 1st as example). For each month, the number of days exceeding the 90th percentile or less than the 10th percentile are calculated in PERT and in CTRL and are finally weighted by the number of calendar days in this same month (divided by 31 days in August for instance). Finally, the difference between the percentage of days in a month exceeding the threshold in PERT and in CTRL is computed. The other indices are also determined for CTRL and PERT to be able to compare both simulations and to understand the effect of sea ice loss on the extremes.

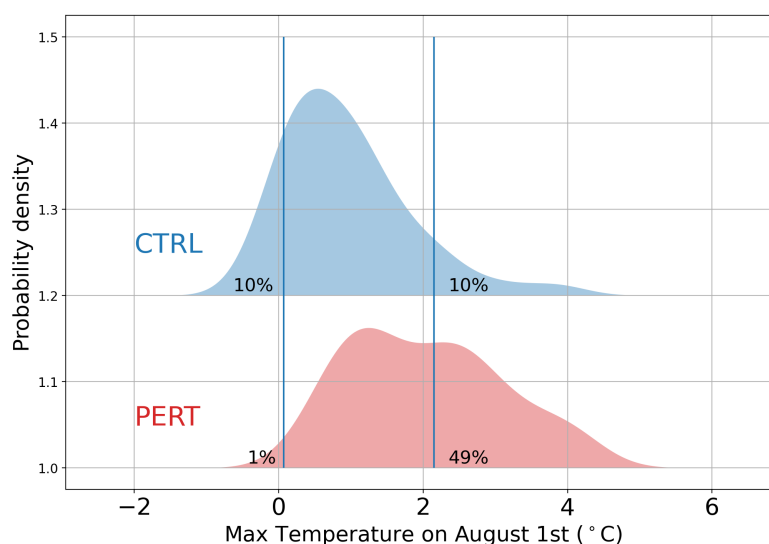


Figure 1. Probability density function of the maximum surface air temperature over Svalbard in CTRL (blue) and in PERT (red) on August 1st. The left and right vertical blue lines show the 10th and 90th percentiles of the CTRL on a 5 day window, respectively. The percentage next to the vertical lines indicates the frequency of days exceeding the 10th (left) and the 90th (right) percentiles of the CTRL.

2.4 Studied areas

Different Arctic regions are considered according to the definitions given in Table 2. Note that when performing spatial averaging, the latitudinal variation in grid cell area is taken into account by weighting the values by the cosine of the latitude.



Table 2. Latitude-longitude range of each region.

Region	Latitude	Longitude
Alaska (AL)	60° N-71° N	169° W-141° W
Northern Canada (NC)	60° N-83° N	141° W-63° W
Greenland (GR)	60° N-83° N	63° W-27° W
Iceland (IC)	63° N-67° N	25° W-12° W
Scandinavia (SC)	60° N-71° N	4°E-30° E
Svalbard (SV)	76° N-81° N	10° E-27° E
Western Russia (WR)	60° N-73° N	30° E-75° E
Eastern Russia (ER)	60° N-77° N	75° E-170° W

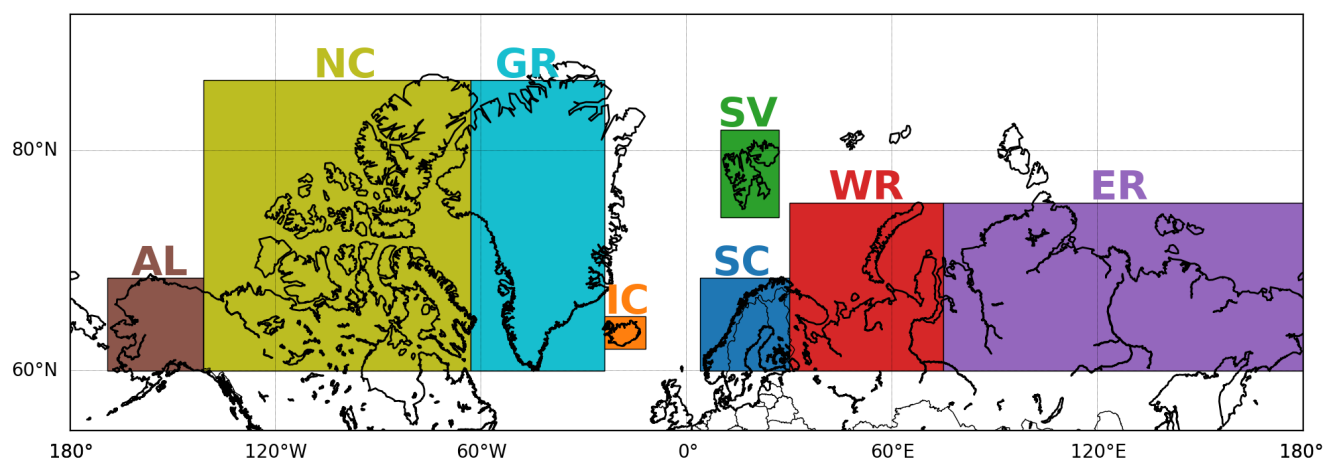


Figure 2. Regions considered in this study. AL stands for Alaska, NC for northern Canada, GR for Greenland, IC for Iceland, SC for Scandinavia, SV for Svalbard, WR for western Russia and ER for eastern Russia.

183 3 Results and discussion

184 3.1 Sea ice loss

185 The seasonality of Arctic sea ice extent in CTRL is well represented for all models with a minimum in September and a max-
 186 imum in February/March (Fig. 3). However, sea ice extent is overestimated throughout the year in ECMWF-LR, while it fits
 187 well with the 1950s observations with a sea ice extent around 16 and 8 millions km² in March and September respectively
 188 (e.g. Onarheim et al., 2018) in the other models. The prescribed drastic change in sea ice albedo (PERT) induces a significant



189 reduction in Arctic sea ice extent, peaking in summer (Figs. 3 and 4).

190

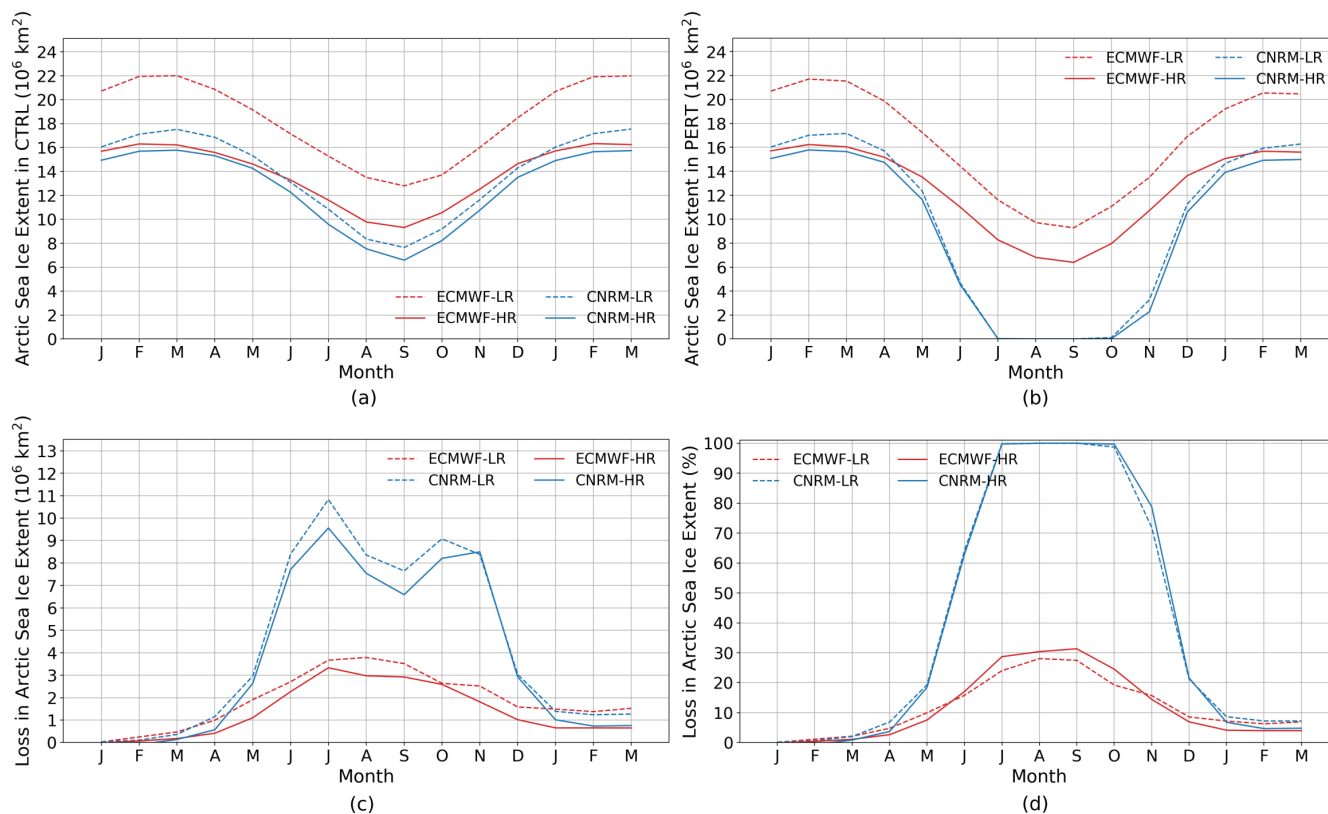


Figure 3. Arctic sea ice extent (in 10^6 km^2) in CTRL (a) and in PERT (b). (c) and (d) show the decrease in Arctic sea ice extent in PERT compared to CTRL (i.e. CTRL - PERT) in 10^6 km^2 and in % relative to the CTRL value, respectively.

191 The induced sea ice loss in these experiments depends on the model used even if the same protocol has been applied. The
 192 decrease in summer Arctic sea ice extent in PERT compared to CTRL reaches 30% for the two ECMWF model configura-
 193 tions, and is largely localized in the eastern Arctic. In the CNRM models, it reaches up to 100% and it is associated with a total
 194 disappearance of sea ice (Figs. 3d and 4). The main reason for these discrepancies is a significant difference in mean sea ice
 195 state between the models, with a large mean sea ice thickness (Docquier et al., 2019) and relatively low ocean heat transport in
 196 the ECMWF configurations (Roberts et al., 2018; Docquier et al., 2019), which could lead to more sea ice in this model.

197

198 The sea ice loss also depends on the horizontal resolution, albeit weakly. More absolute sea ice loss is indeed simulated in
 199 the low resolution models (Fig. 3c). This might be due to larger Arctic sea ice extent in CTRL at lower resolution, particularly
 200 in the Atlantic sector of the Arctic Ocean (Figs. 3a and 4). A higher ocean resolution generally leads to a decrease in sea
 201 ice extent and volume in CTRL in several GCMs used in the PRIMAVERA project due to enhanced poleward oceanic heat

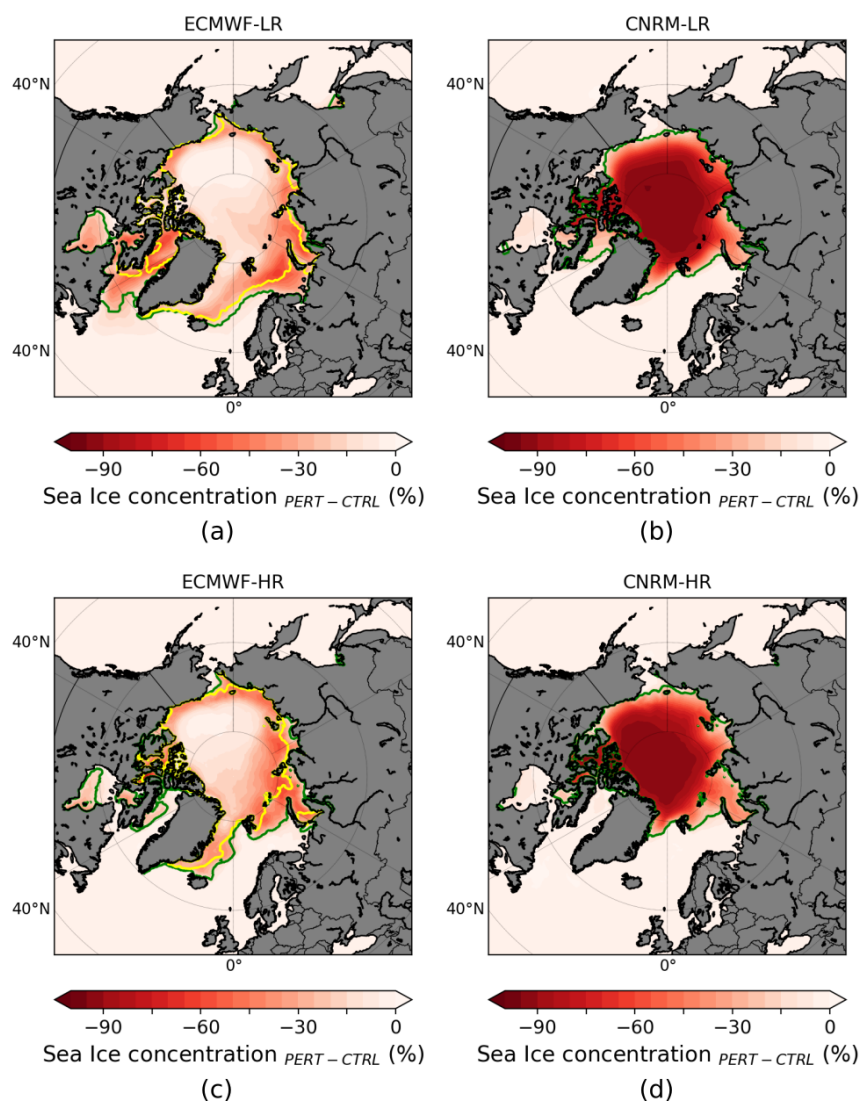


Figure 4. Arctic sea ice concentration change (PERT-CTRL) in summer (JAS) in ECMWF-LR (a) and CNRM-LR (b). (c-d) as (a-b) but for models at high resolution. The green and yellow lines show the sea ice edge (15% ice concentration) from CTRL and PERT, respectively. Note that for the two CNRM model configurations, no yellow line is present because the sea ice has disappeared in PERT.

202 transport (Docquier et al., 2019).

203



204 3.2 Temperature extremes

205 The impact of Arctic sea ice loss on the maximum surface air temperature is now analysed. Figure 5 shows the response of
 206 maximum daily surface air temperature per million km² of sea ice loss in summer (JAS). As expected, an increase in maximum
 207 daily temperature is found over the Arctic. The warming extends to surrounding continents such as Canada, Scandinavia and
 208 northern Russia. Over high latitudes, the CNRM response is larger than the ECMWF one, even after scaling the response by
 209 the amount of sea ice loss. This could be explained by the insulating effect of sea ice, which still exists in ECMWF due to the
 210 presence of sea ice in PERT in summer, and can limit the warming in that model. The change in horizontal resolution does not
 211 strongly impact the response, except over the southern Labrador Sea in ECMWF. In this model, sea ice is present in that area
 212 in CTRL at low resolution but not at high resolution, leading to a warming in ECMWF-LR that is nearly absent in ECMWF-HR.
 213

214 The probability density function (PDF) of the daily summer maximum temperature is shown in Fig. 6 for eight different
 215 peripheral Arctic regions (defined in Table 2 and Fig. 2). The change in PERT compared to CTRL is stronger in CNRM (Fig.
 216 6) because the response cannot be scaled by the amount of sea ice loss in this figure and CNRM experiences a larger Arctic
 217 sea ice loss than ECMWF (Figs. 3 and 4). A shift to the right of the PDF in PERT compared to CTRL, going hand in hand
 218 with a shift of the mean towards higher values, occurs due to sea ice loss over all the selected regions. Nonetheless, this shift
 219 is not symmetrical for most regions, with a larger shift of the left part of the distribution (low temperatures) compared to the
 220 right part (high temperatures) leading to a change in the shape of the distribution. This means that low maximum surface air
 221 temperatures increase more than high maximum surface air temperatures, in agreement with previous studies focusing on high
 222 latitudes (Kharin et al., 2013; Sillmann et al., 2013a).
 223

224 Furthermore, the magnitude of the warming depends on the region. The warming over Svalbard is obviously stronger than
 225 in other regions as Svalbard is made up of islands surrounded (at least in part) by sea ice in early summer in all models in
 226 CTRL. Thus, the sea ice loss in PERT impacts more easily this region than a continent or a further south island such as Iceland.
 227 Northern Canada, which is composed of hundred of islands surrounded by sea ice, is the second region in terms of warming.
 228 Greenland, although it is an island surrounded by sea ice, experiences less warming than the two last regions because an ice
 229 sheet covers almost the whole island and temperatures are much lower over central Greenland than over other Arctic regions,
 230 which does not lead to an important melt of the ice and could mitigate the maximum surface air temperature response to a
 231 sudden sea ice loss over that region (Figs. 5 and 6). We checked that the warming occurring in Greenland cannot be attributed
 232 to the change in the North Atlantic Oscillation (NAO) index (Fig. A1). Only CNRM-LR displays a negative change in the
 233 NAO, which favors positive temperature anomalies over Greenland (Folland et al., 2009), but this change is small compared
 234 to the variability of the ensemble (Fig. A1). As this index exhibits a high variability, 40 members (and even 80 members by
 235 combining the two resolutions) are not enough to detect a robust response in the NAO index.
 236

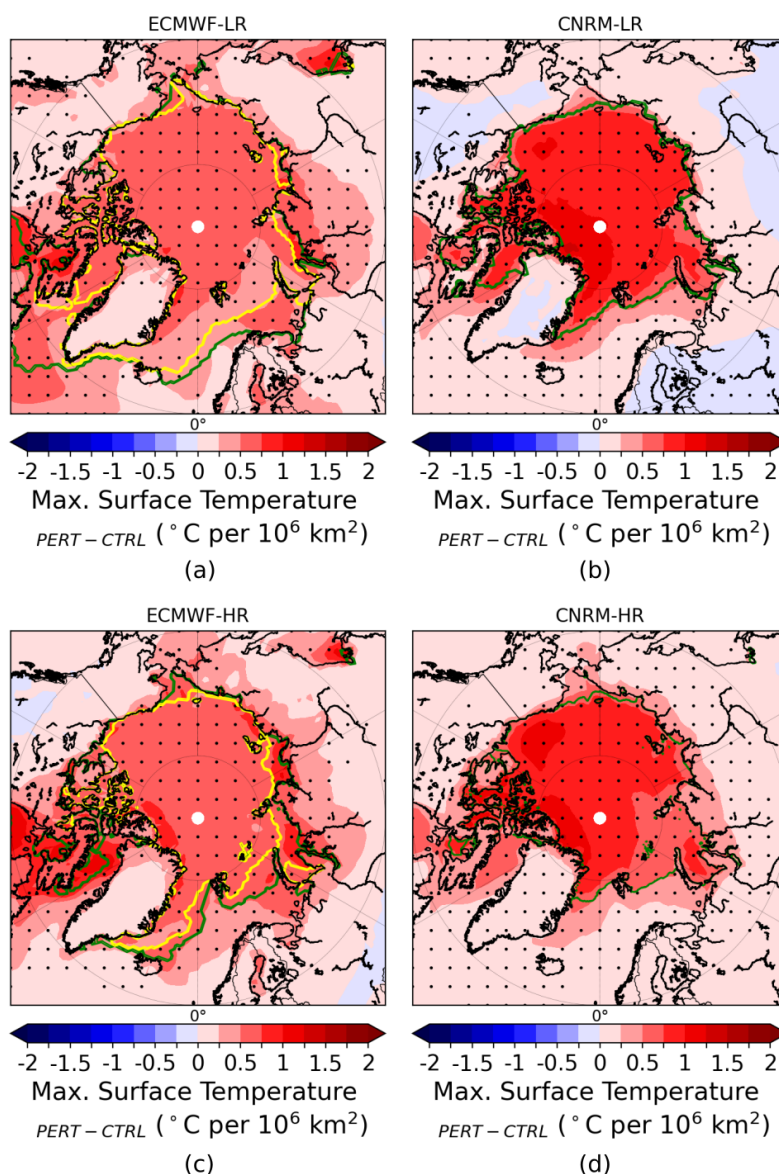


Figure 5. Ensemble mean changes (PERT-CTRL) in maximum daily surface air temperature response over the entire summer (JAS) scaled by the amount of sea ice loss for ECMWF-LR (a), CNRM-LR (b), ECMWF-HR (c) and CNRM-HR (d). The dots show where the response is statistically significant according to a 10% level FDR test associated to a Kolmogorov-Smirnov test. The green and yellow lines represent the sea ice edge (15% ice concentration) from CTRL and PERT, respectively.

237 The increase in maximum surface air temperature over the peripheral Arctic regions is robust although a large internal cli-
 238 mate variability is present. The signal to noise ratio, estimated as the ensemble mean response divided by the standard error,
 239 reveals that the signal exceeds the noise due to internal climate variability over the vast majority of high-latitude regions (Fig.



240 7a). However, in some regions such as western Scandinavia, the center of Greenland, the northwest territories of Canada and
 241 the regions of Russia close to 60° N, the noise exceeds the signal showing that the response is small compared to the role of
 242 internal climate variability even in regions relatively close to the sea ice front.
 243

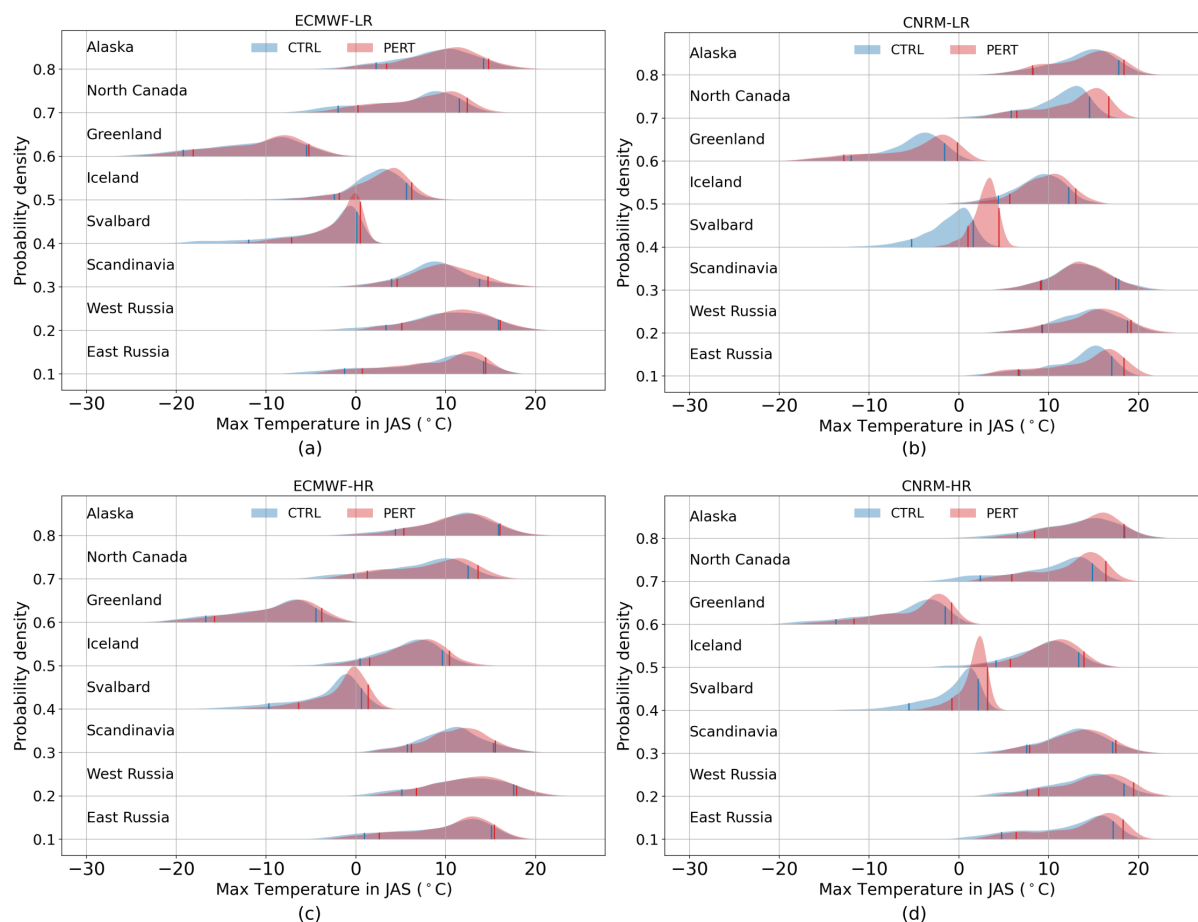


Figure 6. Probability Density Function (PDF) of the daily maximum surface air temperature ($^{\circ}C^{-1}$) in summer (JAS) for ECWMF-LR (a), CNRM-LR (b), ECWMF-HR (c) and CNRM-HR (d). PDF of the CTRL is the blue distribution and PDF of the PERT is the red distribution. The left blue (red) line and the right blue (red) line correspond to the 10th percentile and 90th percentile of the CTRL (PERT), respectively. An offset in Y-axis of 0.1 is taken into account for each region.

244 Figure 8 shows four different temperature extreme indices (see Sect. 2.3) for the eight different regions in summer. As ex-
 245 pected, all regions experience an increase in frequency of warm days (Fig. 8a), a decrease in frequency of cold days (Fig. 8b),
 246 an increase of warm spell duration (Fig. 8c) and a decrease of the number of ice days (Fig. 8d) due to Arctic sea ice loss.
 247 Svalbard exhibits a more drastic change compared to other regions. Indeed, an absolute increase of around 5% (up to 8% in
 248 CNRM-LR) in warm days frequency (Fig. 8a) and also of around 1 day per month (up to 2,5 days per month in CNRM-LR) in

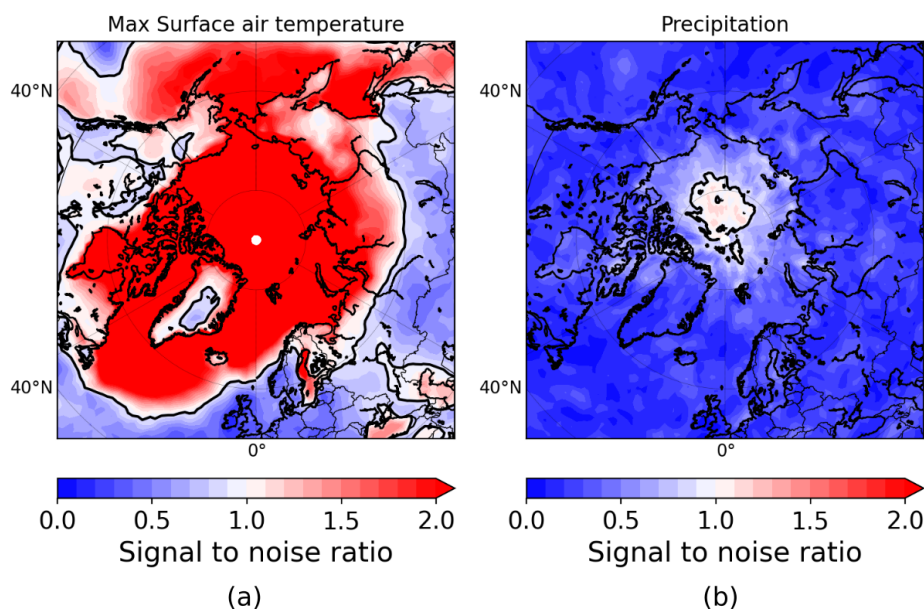


Figure 7. Signal to noise ratio in summer averaged for all the models for the daily maximum surface air temperature (a) and for the daily precipitation (b) responses to summer Arctic sea ice loss. The black line represents where the signal to noise ration is equal to 1.

249 warm spell duration (Fig. 8c) per million km² of sea ice loss are simulated over this region. Furthermore, a loss of one million
 250 km² of sea ice leads to a reduction of at least one ice day per month in Svalbard (Fig. 8d). This is twice as much as the second
 251 region, northern Canada. Other regions experience less intense change in frequency or persistence but all models agree on the
 252 sign of the change except over Scandinavia, where CNRM-LR does not simulate an increase in warm days frequency or in
 253 warm spell duration (Figs. 8a and 8c). These results cannot be directly compared to those of the idealized atmospheric general
 254 circulation model simulations forced by projected Arctic sea ice loss of Screen et al. (2015) because, in the latter study, the
 255 response is not scaled by the amount of sea ice loss, the oceanic areas are taken into account and the response is averaged over
 256 an entire year.

257

258 The maximum daily surface air temperature increase is larger in autumn (not shown), even if the sea ice loss is smaller than
 259 in summer (see Fig. 3), because the turbulent heat flux response is enhanced in autumn due to a large contrast between the
 260 air and surface temperatures during this season (e.g. Deser et al., 2010). However, the increase in the frequency of warm days
 261 are larger in summer over peripheral Arctic regions (not shown), highlighting the importance to study the response of extreme
 262 events during this season. Finally, all extreme indices studied here show a significant increase mainly localized over the Arctic
 263 Ocean, which hardly extends over continents (not shown). Nonetheless, the change in extreme frequency extends more easily
 264 towards continents than the change in extreme persistence.

265

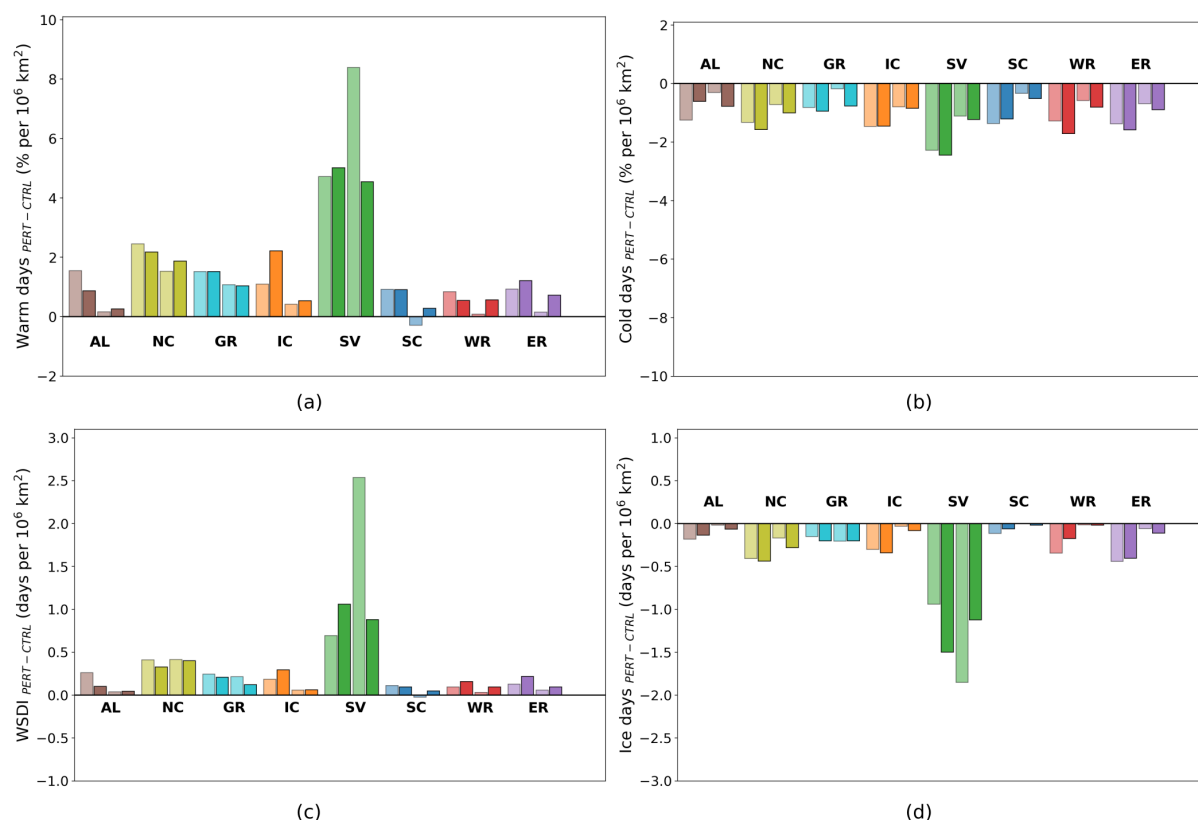


Figure 8. Ensemble mean changes (PERT-CTRL) per month averaged in summer (JAS) in warm days (a), cold days (b), warm spell duration index (c) and ice days (d) scaled by the amount of sea ice loss for the eight regions defined in Table 2 (Fig. 2) for ECMWF-LR (left light bar), ECMWF-HR (left dark bar), CNRM-LR (right light bar) and CNRM-HR (right dark bar).

266 3.3 Precipitation extremes

267 We now investigate the precipitation response with Fig. 9, which shows the monthly mean precipitation response to sea ice loss
 268 in summer. An increase in precipitation is found over the Arctic, which is only statistically significant in CNRM. Newly-open
 269 waters lead to an increase in evaporation, resulting in enhanced precipitation there, in agreement with previous studies (e.g.
 270 Deser et al., 2010; Semmler et al., 2012; Bintanja and Selten, 2014; Semmler et al., 2016; Smith et al., 2017; England et al.,
 271 2018). However, although little sea ice melts in PERT over Central Arctic in summer in ECMWF, an increase in precipitation,
 272 not statistically significant, is simulated over this region (Fig. 9a,c). Furthermore, an increase in precipitation is also observed
 273 over peripheral Arctic regions, mainly on the far north of continents such as northern Alaska, northern Canada and north-
 274 ern Russia (Fig. 9). Nevertheless, these responses are not statistically significant in all models, emphasizing the small signal
 275 and the greater importance of internal climate variability for this variable compared to surface air temperature (Screen et al.,
 276 2014). Indeed, only the region close to the North Pole experiences a signal larger than the noise for the precipitation response



(Fig. 7b), elsewhere, the response is weak compared to internal variability. Furthermore, even by combining the two resolutions (and having 80 members), the precipitation response is still not statistically significant in peripheral Arctic regions (not shown).

No significant change in net precipitation (P-E) is observed over Central Arctic (Fig. A2) showing that the increase in precipitation is balanced by the increase in local evaporation over that region. However, a decrease in P-E is detected near the continental edges of the Arctic Ocean, which is statistically significant in CNRM (Fig. A2b,d). This highlights the fact that the increase in evaporation is larger than the increase in precipitation, which leads to an increase in ocean surface salinity (not shown) despite the melting sea ice in these areas.

The PDF of the daily precipitation in summer is shown in Fig. 10. As for the maximum surface air temperature response (Fig. 6), a shift to the right of the PDF in PERT, reflecting an increase in precipitation, occurs in some regions due to sea ice loss. Nonetheless, the shift is weaker in the daily precipitation response (Fig. 10) than in the daily maximum surface air temperature response (Fig. 6). The change in the distribution between CTRL and PERT seems to be symmetrical in all regions except in Svalbard in CNRM where a small change in the shape of the distribution is observed.

As for the maximum surface air temperature (Fig. 6), the shift is larger in CNRM due to the greater loss of sea ice (Fig. 10) leading to a greater surface heat flux change in this model than in ECMWF (not shown), and can explain the larger response in precipitation in CNRM. Moreover, the increase in precipitation is also stronger in Svalbard and in the northern Canada because these regions are made up of islands surrounded by sea ice, which melts in PERT. Newly-open waters are observed in these regions and lead to a significant increase in precipitation. Furthermore, surface waters are warmer in PERT and generates more evaporation. Finally, as the surface air temperature increases in PERT, the water vapor content increases and can therefore potentially generates more precipitation. In all other regions, the shift to the right of the precipitation distribution is rather weak (Fig. 10), as only the extreme north of each region, close to the Arctic Ocean, experiences an increase in precipitation (Fig. 9). If we now compare the resolutions, no significant differences occur between the LR and the HR.

Figure 11 shows four different precipitation extreme indices (see Sect. 2.3) for the regions in the peripheral Arctic in summer. An increase in the intensity of precipitation extreme is simulated in all regions (Fig. 11a,b). If we average all the models, Svalbard is still the region with the largest increase in intensity of precipitation (Fig. 11a,b). However, other regions further south, such as Iceland or Scandinavia, experience an increase in intensity which can be larger than in Svalbard in some models when the very wet days in a month are summed up (Fig. 11b). Regions over Russia display less significant changes, mainly in the maximum 1 day precipitation indice (Fig. 11a).

The change in persistence of extreme precipitation over the different regions (Fig. 11c,d), mainly in consecutive dry days (Fig. 11c), is not as consistent as the change in magnitude (Fig. 11a,b). Several regions, such as Greenland, Iceland, Scandinavia and western Russia, have a different sign in the response in the consecutive dry days duration to sea ice loss (Fig. 11c).

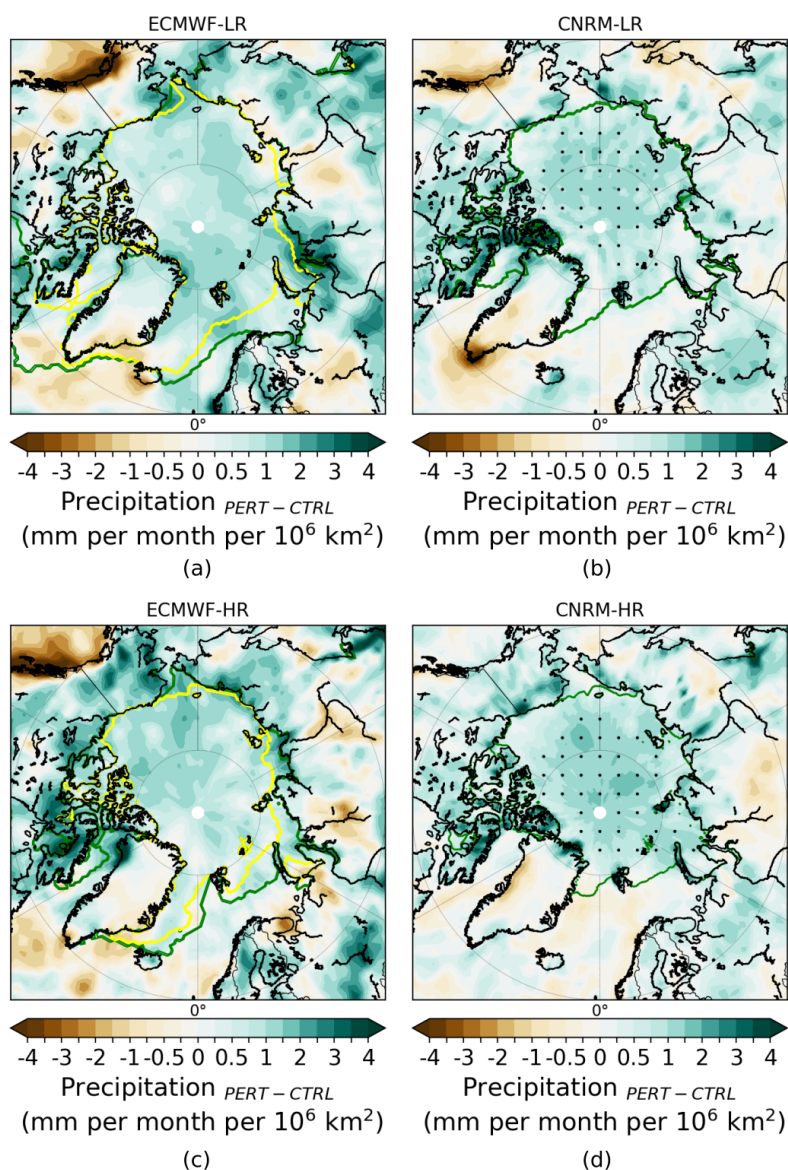


Figure 9. Ensemble mean changes (PERT-CTRL) in summer (JAS) precipitation scaled by the amount of sea ice loss for ECWMF-LR (a), CNRM-LR (b), ECWMF-HR (c) and CNRM-HR (d). The dots show where the response is statistically significant according to a 10% level FDR test associated to a Kolmogorov-Smirnov test. The green and yellow lines represent the sea ice edge (15% ice concentration) from CTRL and PERT, respectively.

312 In the other regions, all models show a decrease in the number of consecutive dry days. Nonetheless, the change in consecutive
 313 wet days duration is more consistent among the regions and the models through an increase in at least 3 of the 4 models for all
 314 regions except in Greenland (Fig. 11d). Therefore, an increase in magnitude but not in persistence is observed over this latter

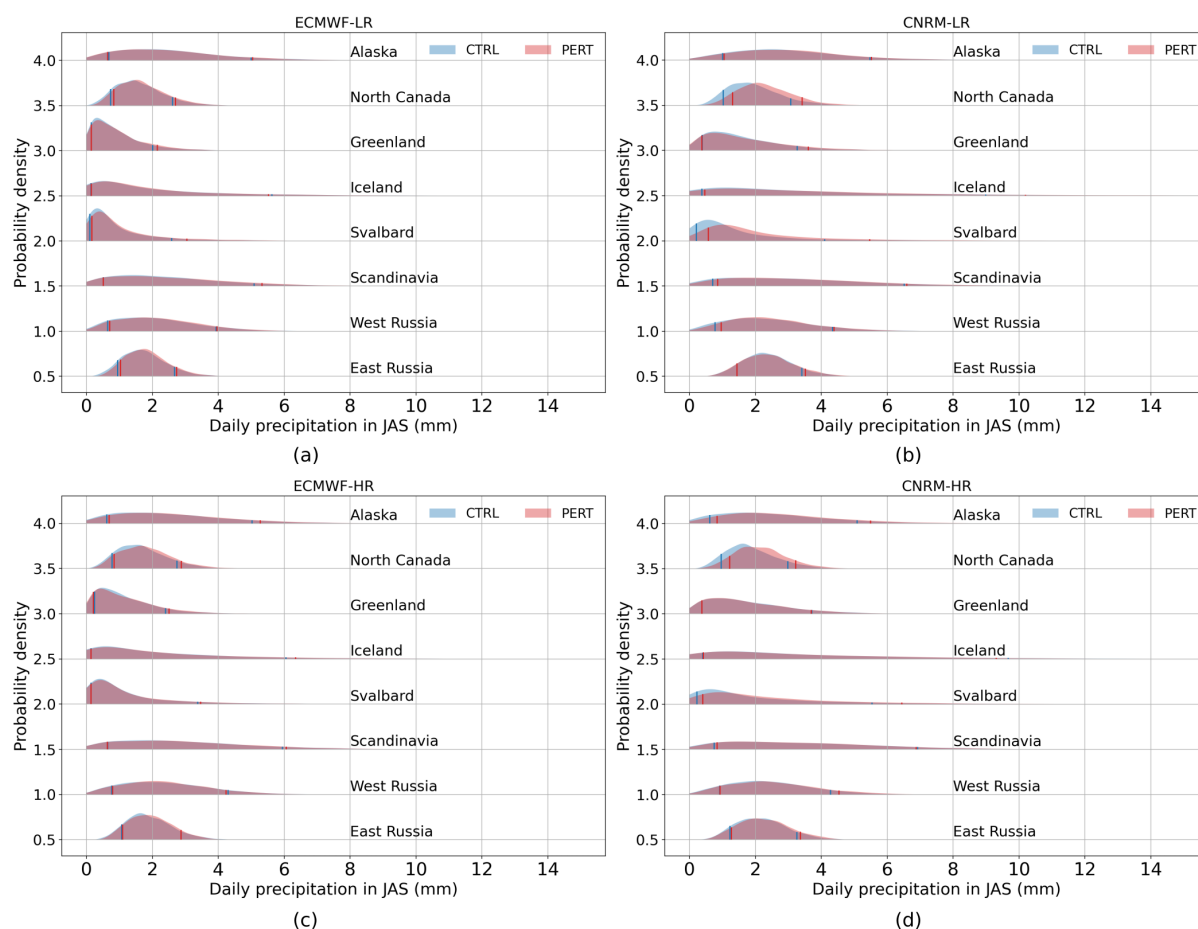


Figure 10. PDF of the daily precipitation in summer (JAS) for ECMWF-LR (a), CNRM-LR (b), ECMWF-HR (c) and CNRM-HR (d). PDF of the CTRL is the blue distribution and PDF of the PERT is the red distribution. The left blue (red) line and the right blue (red) line correspond to the 10th percentile and 90th percentile of the CTRL (PERT), respectively. An offset in Y-axis of 0.5 is taken into account for each region.

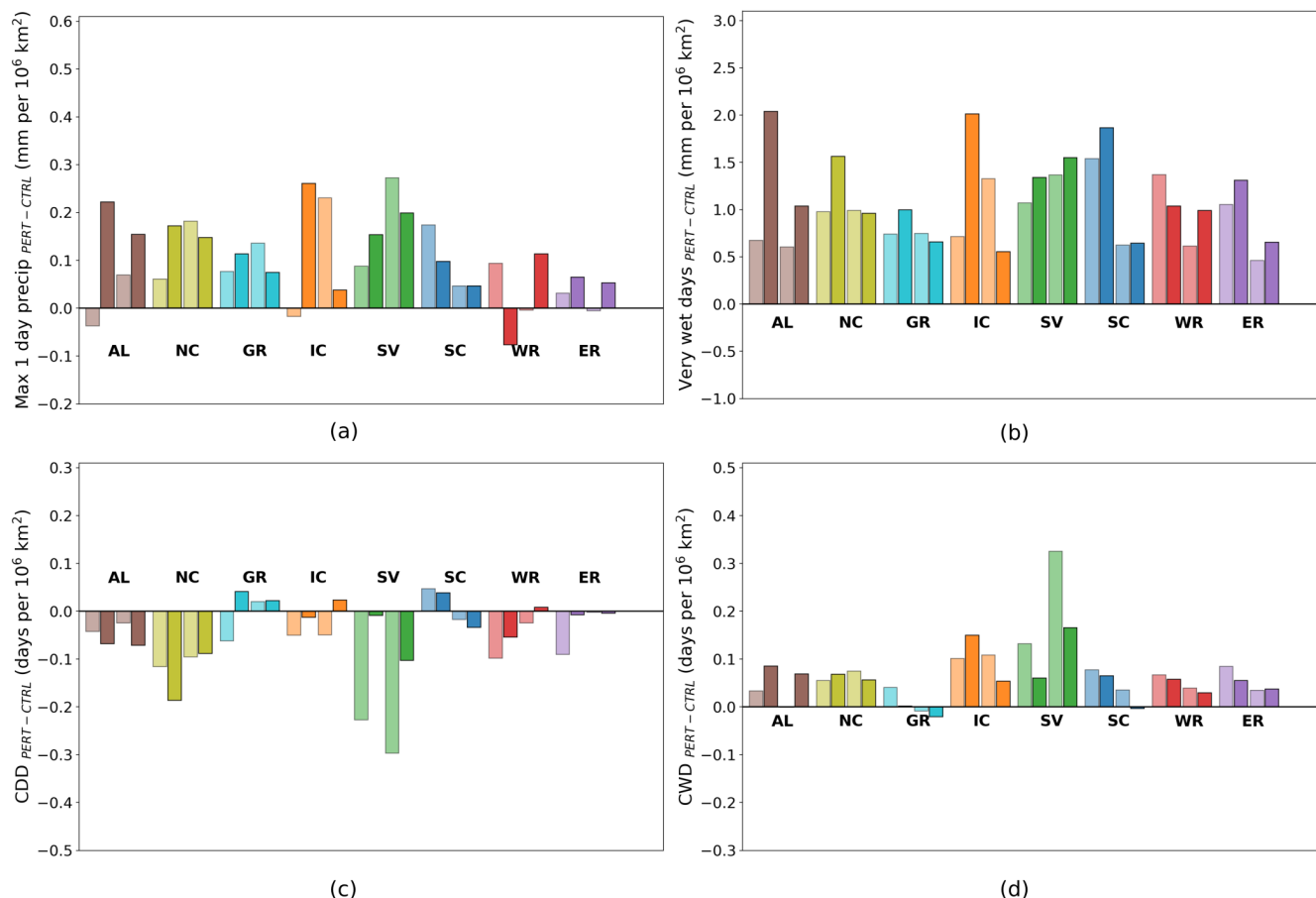


Figure 11. Ensemble mean changes (PERT-CTRL) per month in summer (JAS) in maximum one day precipitation (a), very wet days (b), consecutive dry days (c) and consecutive wet days (d) scaled by the amount of sea ice loss for the eight regions (Fig. 2) for ECMWF-LR (left light bar), ECMWF-HR (left dark bar), CNRM-LR (right light bar) and CNRM-HR (right dark bar). The response is scaled by the amount of the summer Arctic sea ice loss.

315 region. The larger change in magnitude than in persistence of extreme precipitation could be related to the lack of a significant
 316 circulation change (e.g. Fig. A1). Over Svalbard, a decrease in consecutive dry days duration and an increase in consecutive
 317 wet days duration of up to 0.3 days per million km 2 of sea ice loss is modelled in CNRM-LR (Fig. 11c,d), but is weaker in the
 318 other models. Finally, the response in persistence of extreme precipitation remains more restricted to the Arctic Ocean (Fig.
 319 12) than the response in monthly mean precipitation (Fig. 9).

320

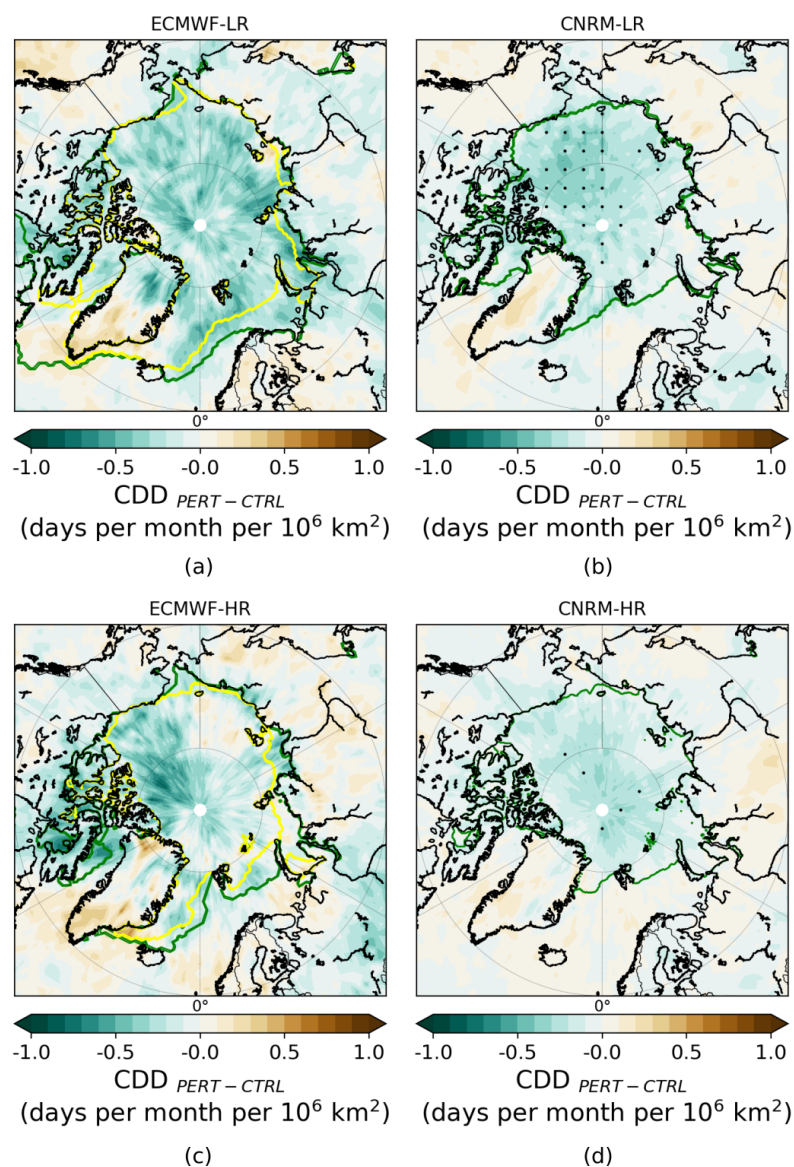


Figure 12. Ensemble mean changes (PERT-CTRL) in summer (JAS) consecutive dry days duration scaled by the amount of sea ice loss in ECMWF-LR (a), CNRM-LR (b), ECMWF-HR (c) and CNRM-HR (d). The dots show where the response is statistically significant according to a 10% level FDR test associated to a Kolmogorov-Smirnov test. The green and yellow lines represent the sea ice edge (15% ice concentration) for CTRL and PERT, respectively.



321 4 Conclusions

322 As the Arctic sea ice continues its decline throughout the century, its variability is projected to increase (e.g. Goosse et al.,
 323 2009). Observing a drastic summer sea ice retreat for one particular year becomes a distinct possibility, yet the consequences
 324 of such an event on the atmosphere have not been deeply explored. The summertime changes in temperature and precipitation
 325 extremes over the peripheral Arctic regions after a sudden sea ice retreat was investigated here. To our knowledge, this study
 326 is the first one to address this last question in depth following a coordinated (fully coupled) two-model approach in which
 327 idealized experiments have been conducted by reducing the sea ice albedo to the ocean value. This protocol helps to isolate as
 328 much as possible the effect of the Arctic sea ice loss without confounding factors.

329

330 During the summer with a strong decline in Arctic sea ice extent, an increase in frequency and persistence of the maximum
 331 surface air temperature occurs over all the peripheral Arctic regions. This increase is especially large in regions made up of
 332 islands surrounded by sea ice in CTRL such as Svalbard or the northern Canada. Svalbard experiences the largest change with
 333 an increase of more than 4% (per million km² of sea ice loss) in the frequency of warm days and of around 1 day (per million
 334 km² of sea ice loss) in warm spell duration index. Over all regions, the low maximum temperatures (cold days) increase more
 335 than the high maximum temperatures (warm days) in summer in response to sea ice loss.

336

337 An increase in extreme precipitation is also found over the peripheral Arctic regions. Nonetheless, the change in precipita-
 338 tion is smaller and less significant than the change in maximum surface air temperature. Furthermore, the response in extreme
 339 precipitation remains more restricted to the Arctic Ocean than the response in mean precipitation. Consistent with the tem-
 340 perature response, Svalbard shows again the largest change, with a decrease in consecutive dry days duration and an increase
 341 in consecutive wet days duration of 0.3 days (per million km² of sea ice loss) in CNRM-LR. However, an increase in the
 342 magnitude of precipitation occurs in all the peripheral Arctic regions in all models.

343

344 The increase in extreme precipitation is found in all the peripheral regions but is relatively small compared to internal climate
 345 variability. For the maximum surface air temperature, the signal exceeds the noise in the majority of the regions north of 60°
 346 N. Even if the two models (ECMWF and CNRM) experience different Arctic sea ice loss, both show a change (scaled by the
 347 amount of sea ice loss) relatively similar in maximum surface air temperature and precipitation, suggesting that the response
 348 over the peripheral Arctic regions evolves about linearly with respect to the amount of sea ice loss. This shows the low impor-
 349 tance of the role of the dynamical response, which tends to be non-linear (Petoukhov and Semenov, 2010), compared to the
 350 role of the thermodynamical response in high latitudes. However, a stronger sea ice loss probably produces a larger statistically
 351 significant response even when the response is scaled by the amount of sea ice loss. Finally, using a higher horizontal resolution
 352 does not considerably affect the response on extreme maximum surface temperature or precipitation.

353



354 Further studies are encouraged to study the response of climate extremes over Arctic regions to sudden sea ice loss as it can
355 influence local communities (Ford et al., 2008), agriculture (Stevenson et al., 2014) and biodiversity (Hollowed et al., 2013;
356 Haug et al., 2017). More members would be needed to detect robust change in extreme precipitation even at high latitudes.
357 Moreover, it would be interesting to analyse the change in extremes over peripheral Arctic regions in summer with other
358 sensitivity experiments simulating a more realistic seasonal cycle of Arctic sea ice loss and using different sea ice perturbation
359 techniques, such as nudging. In conclusion, it is clear that Arctic sea ice loss alone impacts the extreme events on maximum
360 surface temperature over the peripheral Arctic regions, and efforts such as those previously mentioned would help better
361 quantify these climate impacts on these regions.



362 Appendix A

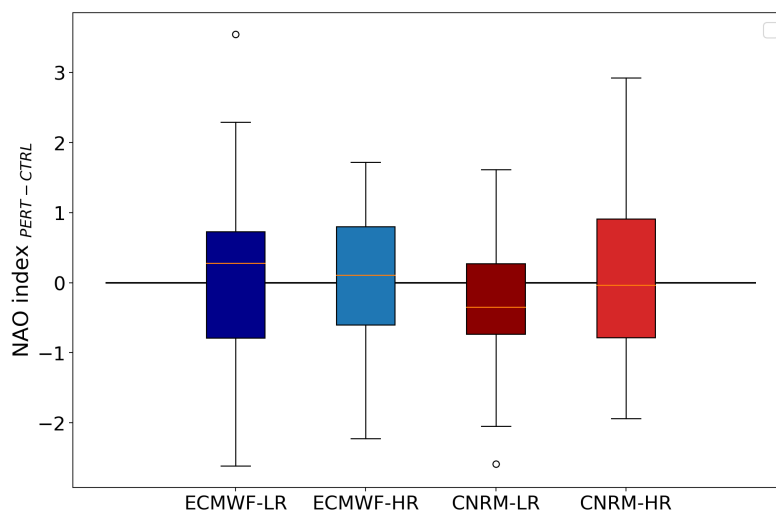


Figure A1. Boxplot of the summer NAO index (station-based method) in PERT compared to CTRL, where the CTRL has been taken as the 40 year reference period, for all members in each model.

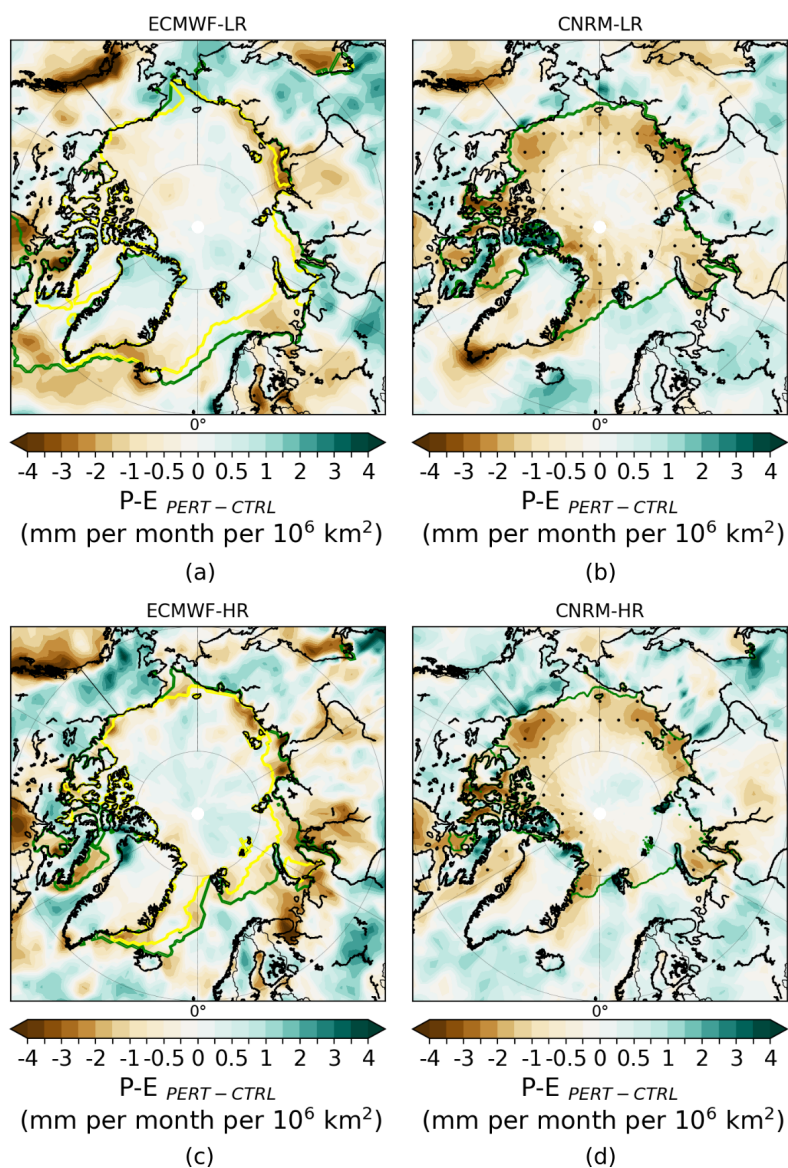


Figure A2. Ensemble mean changes (PERT-CTRL) in summer (JAS) precipitation minus evaporation (P-E) scaled by the amount of sea ice loss for ECWMF-LR (a), CNRM-LR (b), ECWMF-HR (c) and CNRM-HR (d). The dots show where the response is statistically significant according to a 10% level FDR test associated to a Kolmogorov-Smirnov test. The green and yellow lines represent the sea ice edge (15% ice concentration) from CTRL and PERT, respectively.



363 *Author contributions.* SD, TF, FM, RM conceptualized the science plan. RM, SC, CR, SK and RS conducted the experiments. SD performed
364 the analyses, produced the figures and wrote the manuscript based on the insights from the co-authors.

365 *Competing interests.* The authors declare that they have no conflict of interest.

366 *Acknowledgements.* Steve Delhay is F.R.S–FNRS research fellow, Belgium (grant no. 1.A119.20). François Massonnet is a F.R.S.-FNRS
367 Research Associate. Computational resources have been provided by the supercomputing facilities of the Université catholique de Louvain
368 (CISM/UCL) and the Consortium des Équipements de Calcul Intensif en Fédération Wallonie Bruxelles (CÉCI) funded by the Fond de la
369 Recherche Scientifique de Belgique (F.R.S.–FNRS) under convention 2.5020.11. The research leading to these results has received funding
370 from the European Commission’s Horizon 2020 PRIMAVERA (GA 641727) project.



371 References

- 372 Ballinger, T., Overland, J. E., Wang, M., Bhatt, U. S., Hanna, E., Hanssen-Bauer, I., Kim, S.-J., Thoman, R. L., and Walsh, J. E.: Arctic
 373 Report Card 2020: Surface Air Temperature, <https://doi.org/10.25923/GCW8-2Z06>, 2020.
- 374 Balsamo, G., Beljaars, A., Scipal, K., Viterbo, P., van den Hurk, B., Hirschi, M., and Betts, A. K.: A Revised Hydrology for the ECMWF
 375 Model: Verification from Field Site to Terrestrial Water Storage and Impact in the Integrated Forecast System, *Journal of Hydrometeorol-*
 376 *ogy*, 10, 623–643, <https://doi.org/10.1175/2008JHM1068.1>, 2009.
- 377 Barnes, E. A. and Screen, J. A.: The impact of Arctic warming on the midlatitude jet-stream: Can it? Has it? Will it?, *Wiley Interdisciplinary*
 378 *Reviews: Climate Change*, 6, 277–286, <https://doi.org/10.1002/wcc.337>, 2015.
- 379 Benjamini, Y. and Hochberg, Y.: Controlling the false discovery rate: A practical and powerful approach to multiple testing, *J. Roy. Stat.*
 380 *Soc.*, 57B, 289–300, 1995.
- 381 Bintanja, R. and Selten, F. M.: Future increases in Arctic precipitation linked to local evaporation and sea-ice retreat, *Nature*, 509, 479–482,
 382 2014.
- 383 Blackport, R. and Kushner, P. J.: The Transient and Equilibrium Climate Response to Rapid Summertime Sea Ice Loss in CCSM4, *J. Climate*,
 384 29, 401–417, <https://doi.org/10.1175/JCLI-D-15-0284.1>, 2016.
- 385 Blackport, R. and Kushner, P. J.: Isolating the Atmospheric Circulation Response to Arctic Sea Ice Loss in the Coupled Climate System,
 386 *Journal of Climate*, 30, 2163–2185, <https://doi.org/10.1175/JCLI-D-16-0257.1>, 2017.
- 387 Blackport, R. and Screen, J. A.: Insignificant effect of Arctic amplification on the amplitude of midlatitude atmospheric waves, *Science*
 388 *Advances*, 6, <https://doi.org/10.1126/sciadv.aay2880>, 2020.
- 389 Blackport, R., Screen, J. A., van der Wiel, K., and Bintanja, R.: Minimal influence of reduced Arctic sea ice on coincident cold winters in
 390 mid-latitudes, *Nature Climate Change*, 9, 697–704, <https://doi.org/10.1038/s41558-019-0551-4>, 2019.
- 391 Blackport, R., Fyfe, J. C., and Screen, J. A.: Decreasing subseasonal temperature variability in the northern extratropics attributed to human
 392 influence, *Nature Geoscience*, 14, 719–723, <https://doi.org/10.1038/s41561-021-00826-w>, 2021.
- 393 Bouillon, S., Morales Maqueda, M. Á., Legat, V., and Fichet, T.: An elastic-viscous-plastic sea ice model formulated on Arakawa B and C
 394 grids, *Ocean Modelling*, 27, 174–184, <https://doi.org/10.1016/j.ocemod.2009.01.004>, 2009.
- 395 Cohen, J., Screen, J. A., Furtado, J. C., Barlow, M., Whittleston, D., Coumou, D., Francis, J., Dethloff, K., Entekhabi, D., Overland, J., and
 396 Jones, J.: Recent Arctic amplification and extreme mid-latitude weather, *Nat. Geosci.*, 7, 627–637, <http://dx.doi.org/10.1038/ngeo2234>,
 397 2014.
- 398 Cohen, J., Zhang, X., Francis, J., Jung, T., Kwok, R., Overland, J., Ballinger, T. J., Bhatt, U. S., Chen, H. W., Coumou, D., Feldstein,
 399 S., Gu, H., Handorf, D., Henderson, G., Ionita, M., Kretschmer, M., Laliberte, F., Lee, S., Linderholm, H. W., Maslowski, W., Peings,
 400 Y., Pfeiffer, K., Rigor, I., Semmler, T., Stroeve, J., Taylor, P. C., Vavrus, S., Vihma, T., Wang, S., Wendisch, M., Wu, Y., and Yoon,
 401 J.: Divergent consensus on Arctic amplification influence on midlatitude severe winter weather, *Nature Climate Change*, 10, 20–29,
 402 <https://doi.org/10.1038/s41558-019-0662-y>, 2020.
- 403 Cowtan, K. and Way, R. G.: Coverage bias in the HadCRUT4 temperature series and its impact on recent temperature trends, *Quarterly*
 404 *Journal of the Royal Meteorological Society*, 140, 1935–1944, <https://doi.org/10.1002/qj.2297>, 2014.
- 405 Craig, A., Valcke, S., and Coquart, L.: Development and performance of a new version of the OASIS coupler, OASIS3-MCT_3.0, *Geoscientific*
 406 *Model Development*, 10, 3297–3308, <https://doi.org/10.5194/gmd-10-3297-2017>, 2017.



- 407 Dai, A. and Song, M.: Little influence of Arctic amplification on mid-latitude climate, *Nature Climate Change*, 10, 231–237,
408 <https://doi.org/10.1038/s41558-020-0694-3>, 2020.
- 409 Deser, C., Tomas, R., Alexander, M., and Lawrence, D.: The Seasonal Atmospheric Response to Projected Arctic Sea Ice Loss in the Late
410 Twenty-First Century, *J. Climate*, 23, 333–351, <http://dx.doi.org/10.1175/2009JCLI3053.1>, 2010.
- 411 Deser, C., Tomas, R. A., and Sun, L.: The Role of Ocean–Atmosphere Coupling in the Zonal-Mean Atmospheric Response to Arctic Sea Ice
412 Loss, *J. Climate*, 28, 2168–2186, <http://dx.doi.org/10.1175/JCLI4278.1>, 2015.
- 413 Ding, Q., Schweiger, A., L’Heureux, M., Battisti, D., Po-Chedley, S., Johnson, N., Blanchard-Wrigglesworth, E., Harnos, K., Zhang, Q.,
414 Eastman, R., and Steig, E.: Influence of high-latitude atmospheric circulation changes on summertime Arctic sea ice, *Nature Clim. Change*,
415 7, 289–295, 2017.
- 416 Docquier, D., Grist, J. P., Roberts, M. J., Roberts, C. D., Semmler, T., Ponsoni, L., Massonnet, F., Sidoreno, D., Sein, D. V., Iovino, D.,
417 Bellucci, A., and Fichefet, T.: Impact of model resolution on Arctic sea ice and North Atlantic Ocean heat transport, *Climate Dynamics*,
418 53, 4989–5017, <https://doi.org/10.1007/s00382-019-04840-y>, 2019.
- 419 England, M., Polvani, L., and Sun, L.: Contrasting the Antarctic and Arctic Atmospheric Responses to Projected Sea Ice Loss in the Late
420 Twenty-First Century, *Journal of Climate*, 31, 6353–6370, <https://doi.org/10.1175/JCLI-D-17-0666.1>, 2018.
- 421 Eyring, V., Bony, S., Meehl, G. A., Senior, C. A., Stevens, B., Stouffer, R. J., and Taylor, K. E.: Overview of the Coupled Model
422 Intercomparison Project Phase 6 (CMIP6) experimental design and organization, *Geoscientific Model Development*, 9, 1937–1958,
423 <https://doi.org/10.5194/gmd-9-1937-2016>, 2016.
- 424 Fichefet, T. and Morales Maqueda, M. : Sensitivity of a global sea ice model to the treatment of ice thermodynamics and dynamics, *Journal*
425 *of Geophysical Research*, 1021, 12 609–12 646, <https://doi.org/10.1029/97JC00480>, 1997.
- 426 Folland, C. K., Knight, J., Linderholm, H. W., Fereday, D., Ineson, S., and Hurrell, J. W.: The Summer North Atlantic Oscillation: Past,
427 Present, and Future, *Journal of Climate*, 22, 1082–1103, <https://doi.org/10.1175/2008JCLI2459.1>, 2009.
- 428 Ford, J. D., Smit, B., Wandel, J., Allurut, M., Shappa, K., Ittusarjuat, H., and Qrunnut, K.: Climate change in the Arctic: current and future
429 vulnerability in two Inuit communities in Canada, *The Geographical Journal*, 174, 45–62, [https://doi.org/https://doi.org/10.1111/j.1475-](https://doi.org/https://doi.org/10.1111/j.1475-4959.2007.00249.x)
430 [4959.2007.00249.x](https://doi.org/https://doi.org/10.1111/j.1475-4959.2007.00249.x), 2008.
- 431 Francis, J. A.: Why Are Arctic Linkages to Extreme Weather Still up in the Air?, *Bulletin of the American Meteorological Society*, 98, 2551
432 – 2557, <https://doi.org/10.1175/BAMS-D-17-0006.1>, 2017.
- 433 Francis, J. A. and Vavrus, S. J.: Evidence linking Arctic amplification to extreme weather in mid-latitudes, *Geophys. Res. Lett.*, 39, L06 801,
434 2012.
- 435 Goosse, H., Arzel, O., Bitz, C. M., de Montety, A., and Vancoppenolle, M.: Increased variability of the Arctic summer ice extent in a warmer
436 climate, *Geophysical Research Letters*, 36, <https://doi.org/10.1029/2009GL040546>, 2009.
- 437 Haarsma, R. J., Roberts, M. J., Vidale, P. L., Senior, C. A., Bellucci, A., Bao, Q., Chang, P., Corti, S., Fučkar, N. S., Guemas, V., von Harden-
438 berg, J., Hazeleger, W., Kodama, C., Koenigk, T., Leung, L. R., Lu, J., Luo, J.-J., Mao, J., Mizielinski, M. S., Mizuta, R., Nobre, P., Satoh,
439 M., Scoccimarro, E., Semmler, T., Small, J., and von Storch, J.-S.: High Resolution Model Intercomparison Project (HighResMIP v1.0)
440 for CMIP6, *Geoscientific Model Development*, 9, 4185–4208, <https://doi.org/10.5194/gmd-9-4185-2016>, 2016.
- 441 Haug, T., Bogstad, B., Chierici, M., Gjøsæter, H., Hallfredsson, E. H., Åge S. Høines, Hoel, A. H., Ingvaldsen, R. B., Jørgensen,
442 L. L., Knutsen, T., Loeng, H., Naustvoll, L.-J., Røttingen, I., and Sunnanå, K.: Future harvest of living resources in the Arc-
443 tic Ocean north of the Nordic and Barents Seas: A review of possibilities and constraints, *Fisheries Research*, 188, 38–57,
444 <https://doi.org/https://doi.org/10.1016/j.fishres.2016.12.002>, 2017.



- 445 Holland, M. M., Bitz, C. M., and Tremblay, B.: Future abrupt reductions in the summer Arctic sea ice, *Geophysical Research Letters*, 33,
446 <https://doi.org/10.1029/2006GL028024>, 2006.
- 447 Hollowed, A. B., Planque, B., and Loeng, H.: Potential movement of fish and shellfish stocks from the sub-Arctic to the Arctic Ocean,
448 *Fisheries Oceanography*, 22, 355–370, <https://doi.org/10.1111/fog.12027>, 2013.
- 449 Kharin, V., Zwiers, F., Zhang, X., and Wehner, M.: Changes in temperature and precipitation extremes in the CMIP5 ensemble, *Climatic*
450 *Change*, 119, 345–357, <https://doi.org/10.1007/s10584-013-0705-8>, 2013.
- 451 Kunkel, K. E., Pielke, R. A., and Changnon, S. A.: Temporal Fluctuations in Weather and Climate Extremes That Cause Economic and
452 Human Health Impacts: A Review, *Bulletin of the American Meteorological Society*, 80, 1077 – 1098, [https://doi.org/10.1175/1520-0477\(1999\)080<1077:TFIWAC>2.0.CO;2](https://doi.org/10.1175/1520-0477(1999)080<1077:TFIWAC>2.0.CO;2), 1999.
- 453 Lindsay, R. and Schweiger, A.: Arctic sea ice thickness loss determined using subsurface, aircraft, and satellite observations, *The Cryosphere*,
454 9, 269–283, <https://doi.org/10.5194/tc-9-269-2015>, 2015.
- 455 Madec, G.: NEMO Ocean ocean engine (Note du Pôle de modélisation, Institut Pierre-Simon Laplace (IPSL), France, No 27, ISSN No
456 1288-1619), 2016.
- 457 Madec, G., Benschila, R., Bricaud, C., Coward, A., Dobricic, S., Furner, R., and Oddo, P.: NEMO ocean engine,
458 <https://doi.org/10.5281/zenodo.1464817>, revision 3797 from SVN repository (missing links), 2013.
- 459 Madec, G., Bourdallé-Badie, R., Bouttier, P.-A., Bricaud, C., Bruciaferri, D., Calvert, D., Chanut, J., Clementi, E., Coward, A., Delrosso,
460 D., Ethé, C., Flavoni, S., Graham, T., Harle, J., Iovino, D., Lea, D., Lévy, C., Lovato, T., Martin, N., Masson, S., Mocavero, S., Paul, J.,
461 Rousset, C., Storkey, D., Storto, A., and Vancoppenolle, M.: NEMO ocean engine, <https://doi.org/10.5281/zenodo.1472492>, revision 8625
462 from SVN repository (missing links), 2017.
- 463 Mallett, R. D. C., Stroeve, J. C., Tsamados, M., Landy, J. C., Willatt, R., Nandan, V., and Liston, G. E.: Faster decline and higher vari-
464 ability in the sea ice thickness of the marginal Arctic seas when accounting for dynamic snow cover, *The Cryosphere*, 15, 2429–2450,
465 <https://doi.org/10.5194/tc-15-2429-2021>, 2021.
- 466 Manabe, S. and Stouffer, R. J.: Multiple-Century Response of a Coupled Ocean-Atmosphere Model to an Increase of Atmospheric Carbon
467 Dioxide, *Journal of Climate*, 7, 5 – 23, [https://doi.org/10.1175/1520-0442\(1994\)007<0005:MCROAC>2.0.CO;2](https://doi.org/10.1175/1520-0442(1994)007<0005:MCROAC>2.0.CO;2), 1994.
- 468 Masson, V., Le Moigne, P., Martin, E., Faroux, S., Alias, A., Alkama, R., Belamari, S., Barbu, A., Boone, A., Bouysse, F., Brousseau, P.,
469 Brun, E., Calvet, J.-C., Carrer, D., Decharme, B., Delire, C., Donier, S., Essaouini, K., Gibelin, A.-L., Giordani, H., Habets, F., Jidane, M.,
470 Kerdraon, G., Kourzeneva, E., Lafaysse, M., Lafont, S., Lebeaupin Brossier, C., Lemonsu, A., Mahfouf, J.-F., Marguinaud, P., Mokhtari,
471 M., Morin, S., Pigeon, G., Salgado, R., Seity, Y., Taillefer, F., Tanguy, G., Tulet, P., Vincendon, B., Vionnet, V., and Voldoire, A.: The
472 SURFEXv7.2 land and ocean surface platform for coupled or offline simulation of earth surface variables and fluxes, *Geoscientific Model*
473 *Development*, 6, 929–960, <https://doi.org/10.5194/gmd-6-929-2013>, 2013.
- 474 Mogensen, K., Keeley, S., and Towers, P.: Coupling of the NEMO and IFS models in a single executable, p. 23, 2012.
- 475 Mori, M., Watanabe, M., Shiogama, H., Inoue, J., and Kimoto, M.: Robust Arctic sea-ice influence on the frequent Eurasian cold winters in
476 past decades, *Nature Geoscience*, 7, 869–873, <https://doi.org/10.1038/NGEO2277>, 2014.
- 477 Notz, D. and Stroeve, J.: Observed Arctic sea-ice loss directly follows anthropogenic CO₂ emission, *Science*, 354, 747–750,
478 <https://doi.org/10.1126/science.aag2345>, 2016.
- 479 Ogawa, F., Keenlyside, N., Gao, Y., Koenigk, T., Yang, S., Suo, L., Wang, T., Gastineau, G., Nakamura, T., Cheung, H. N., Omrani, N.-
480 E., Ukita, J., and Semenov, V.: Evaluating Impacts of Recent Arctic Sea Ice Loss on the Northern Hemisphere Winter Climate Change,
481 *Geophysical Research Letters*, 45, 3255–3263, <https://doi.org/10.1002/2017GL076502>, 2018.



- Onarheim, I. H., Eldevik, T., Smedsrud, L. H., and Stroeve, J. C.: Seasonal and Regional Manifestation of Arctic Sea Ice Loss, *Journal of Climate*, 31, 4917–4932, <https://doi.org/10.1175/JCLI-D-17-0427.1>, 2018.
- Park, H.-S., Kim, S.-J., Seo, K.-H., Stewart, A. L., Kim, S.-Y., and Son, S.-W.: The impact of Arctic sea ice loss on mid-Holocene climate, *Nature Communications*, 9, 2018.
- Peings, Y., Labe, Z. M., and Magnusdottir, G.: Are 100 Ensemble Members Enough to Capture the Remote Atmospheric Response to +2°C Arctic Sea Ice Loss?, *Journal of Climate*, 34, 3751 – 3769, <https://doi.org/10.1175/JCLI-D-20-0613.1>, 2021.
- Petoukhov, V. and Semenov, V. A.: A link between reduced Barents-Kara sea ice and cold winter extremes over northern continents, *Journal of Geophysical Research: Atmospheres*, 115, <https://doi.org/10.1029/2009JD013568>, 2010.
- Pithan, Y. and Mauritsen, T.: Arctic amplification dominated by temperature feedbacks in contemporary climate models, *Nature Geoscience*, 7, 181–184, <https://doi.org/10.1175/JCLI-D-13-00272.1>, 2014.
- Ritchie, H., Temperton, C., Simmons, A., Hortal, M., Davies, T., Dent, D., and Hamrud, M.: Implementation of the semi-Lagrangian method in a high-resolution version of the ECMWF forecast model, *Weather Rev*, 123, 489–514, 1995.
- Roberts, C. D., Senan, R., Molteni, F., Boussetta, S., Mayer, M., and Keeley, S. P. E.: Climate model configurations of the ECMWF Integrated Forecasting System (ECMWF-IFS cycle 43r1) for HighResMIP, *Geoscientific Model Development*, 11, 3681–3712, <https://doi.org/10.5194/gmd-11-3681-2018>, 2018.
- Screen, J., Deser, C., Simmonds, I., and Tomas, R.: Atmospheric impacts of Arctic sea-ice loss, 1979–2009: separating forced change from atmospheric internal variability, 43, 333–344–, <http://dx.doi.org/10.1007/s00382-013-1830-9>, 2014.
- Screen, J. A. and Simmonds, I.: The central role of diminishing sea ice in recent Arctic temperature amplification, *Nature*, 464, 1334–1337, 2010.
- Screen, J. A., Deser, C., and Sun, L.: Projected changes in regional climate extremes arising from Arctic sea ice loss, *Environmental Research Letters*, 10, 084 006, <https://doi.org/10.1088/1748-9326/10/8/084006>, 2015.
- Screen, J. A., Deser, C., Smith, D. M., Zhang, X., Blackport, R., Kushner, P. J., Oudar, T., McCusker, K. E., 6, and Sun, L.: Consistency and discrepancy in the atmospheric response to Arctic sea-ice loss across climate models, *Nat. Geosci.*, 11, 155–163, doi: 10.1038/s41561-018-0059-y, 2018.
- Semmler, T., McGrath, R., and Wang, S.: The impact of Arctic sea ice on the Arctic energy budget and on the climate of the Northern mid-latitudes, *Climate Dynamics*, 39, 2675–2694, <https://doi.org/10.1007/s00382-012-1353-9>, 2012.
- Semmler, T., Stulic, L., Jung, T., Tilinina, N., Campos, C., Gulev, S., and Koracin, D.: Seasonal Atmospheric Responses to Reduced Arctic Sea Ice in an Ensemble of Coupled Model Simulations, *J. Climate*, 29, 5893–5913, <https://doi.org/10.1175/JCLI-D-15-0586.1>, 2016.
- Serreze, M. C., Barrett, A. P., Stroeve, J. C., Kindig, D. N., and Holland, M. M.: The emergence of surface-based Arctic amplification, *The Cryosphere*, 3, 11–19, <https://doi.org/10.5194/tc-3-11-2009>, 2009.
- Sillmann, J., Kharin, V. V., Zhang, X., Zwiers, F. W., and Bronaugh, D.: Climate extremes indices in the CMIP5 multimodel ensemble: Part 1. Model evaluation in the present climate, *J Geophys Res*, 118, 1716–1733, <https://doi.org/10.1002/jgrd.50203>, 2013a.
- Sillmann, J., Kharin, V. V., Zwiers, F. W., Zhang, X., and Bronaugh, D.: Climate extremes indices in the CMIP5 multimodel ensemble: Part 2. Future climate projections, *Journal of Geophysical Research: Atmospheres*, 118, 2473–2493, <https://doi.org/https://doi.org/10.1002/jgrd.50188>, 2013b.
- SIMIP, C.: Arctic Sea Ice in CMIP6, *Geophysical Research Letters*, 47, e2019GL086 749, <https://doi.org/10.1029/2019GL086749>, 2020.



- 519 Smith, D. M., Dunstone, N. J., Scaife, A. A., Fiedler, E. K., Copsey, D., and Hardiman, S. C.: Atmospheric Response to Arc-
520 tic and Antarctic Sea Ice: The Importance of Ocean–Atmosphere Coupling and the Background State, *J. Climate*, 30, 4547–4565,
521 <https://doi.org/10.1175/JCLI-D-16-0564.1>, 2017.
- 522 Smith, D. M., Screen, J. A., Deser, C., Cohen, J., Fyfe, J. C., García-Serrano, J., Jung, T., Kattsov, V., Matei, D., Msadek, R., Peings,
523 Y., Sigmond, M., Ukita, J., Yoon, J.-H., and Zhang, X.: The Polar Amplification Model Intercomparison Project (PAMIP) contribu-
524 tion to CMIP6: investigating the causes and consequences of polar amplification, *Geoscientific Model Development*, 12, 1139–1164,
525 <https://doi.org/10.5194/gmd-12-1139-2019>, 2019.
- 526 Stevenson, K. T., RADER, H. B., ALESSA, L., KLISKEY, A. D., PANTOJA, A., CLARK, M., SMEENK, J., and Giguère, N.: Sustainable
527 Agriculture for Alaska and the Circumpolar North: Part II. Environmental, Geophysical, Biological and Socioeconomic Challenges,
528 *Arctic*, 67, 296–319, 2014.
- 529 Swart, N. C., Fyfe, J. C., Hawkins, E., Kay, J. E., and Jahn, A.: Influence of internal variability on Arctic sea-ice trends, *Nature Climate*
530 *Change*, 5, 86–89, <https://doi.org/10.1038/nclimate2483>, 2015.
- 531 Temperton, C., Hortal, M., and Simmons, A.: A two-time-level semi-Lagrangian global spectral model, pp. 111–127, 2001.
- 532 Voldoire, A., Saint-Martin, D., Sénési, S., Decharme, B., Alias, A., Chevallier, M., Colin, J., Guérémy, J.-F., Michou, M., Moine, M.-P.,
533 Nabat, P., Roehrig, R., Salas y Mélia, D., Séférian, R., Valcke, S., Beau, I., Belamari, S., Berthet, S., Cassou, C., Cattiaux, J., Deshayes,
534 J., Douville, H., Ethé, C., Franchistéguy, L., Geoffroy, O., Lévy, C., Madec, G., Meurdesoif, Y., Msadek, R., Ribes, A., Sanchez-Gomez,
535 E., Terray, L., and Waldman, R.: Evaluation of CMIP6 DECK Experiments With CNRM-CM6-1, *Journal of Advances in Modeling Earth*
536 *Systems*, 11, 2177–2213, <https://doi.org/10.1029/2019MS001683>, 2019.
- 537 Wilks, D. S.: “The Stippling Shows Statistically Significant Grid Points”: How Research Results are Routinely Overstated and Overinter-
538 preted, and What to Do about It, *Bulletin of the American Meteorological Society*, 97, 2263–2273, [https://doi.org/10.1175/BAMS-D-15-](https://doi.org/10.1175/BAMS-D-15-00267.1)
539 [00267.1](https://doi.org/10.1175/BAMS-D-15-00267.1), 2016.
- 540 Zhang, X., Alexander, L., Hegerl, G. C., Jones, P., Tank, A. K., Peterson, T. C., Trewin, B., and Zwiers, F. W.: Indices
541 for monitoring changes in extremes based on daily temperature and precipitation data, *WIREs Climate Change*, 2, 851–870,
542 <https://doi.org/https://doi.org/10.1002/wcc.147>, 2011.